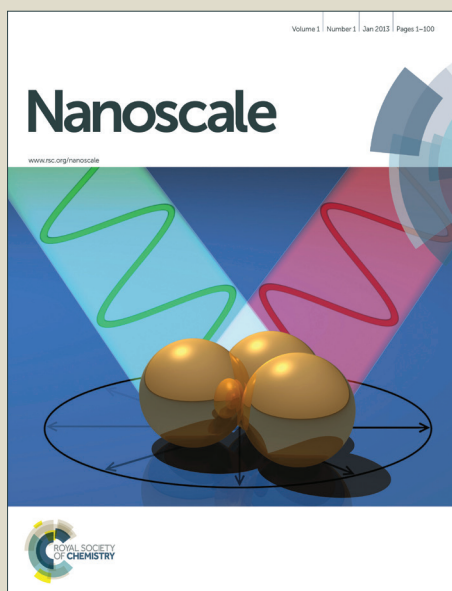


# Nanoscale

Accepted Manuscript



This is an *Accepted Manuscript*, which has been through the Royal Society of Chemistry peer review process and has been accepted for publication.

*Accepted Manuscripts* are published online shortly after acceptance, before technical editing, formatting and proof reading. Using this free service, authors can make their results available to the community, in citable form, before we publish the edited article. We will replace this *Accepted Manuscript* with the edited and formatted *Advance Article* as soon as it is available.

You can find more information about *Accepted Manuscripts* in the [Information for Authors](#).

Please note that technical editing may introduce minor changes to the text and/or graphics, which may alter content. The journal's standard [Terms & Conditions](#) and the [Ethical guidelines](#) still apply. In no event shall the Royal Society of Chemistry be held responsible for any errors or omissions in this *Accepted Manuscript* or any consequences arising from the use of any information it contains.

# Carbon Dioxide Conversion into Hydrocarbon Fuels on Defective Graphene-Supported Cu Nanoparticles from First Principles

Dong-Hee Lim<sup>1)\*</sup>, Jun Ho Jo<sup>1)</sup>, Dong Yun Shin<sup>1)</sup>, Jennifer Wilcox<sup>2)</sup>,  
Hyung Chul Ham<sup>1)</sup>, and Suk Woo Nam<sup>1)</sup>

<sup>1)</sup> Fuel Cell Research Center, Korea Institute of Science and Technology (KIST),  
Hwarangno 14-gil 5, Seongbuk-gu, Seoul 136-791, Republic of Korea

<sup>2)</sup> Department of Energy Resources Engineering, Stanford University  
367 Panama Street, Green Earth Sciences, Stanford, CA 94305-2220, USA

(\* Corresponding author: limkr@kist.re.kr)

Author Email Addresses:

Dong-Hee Lim (limkr@kist.re.kr), Jun Ho Jo (galer821@gmail.com),  
Dong Yun Shin (84sindy@gmail.com), Jennifer Wilcox (wilcoxj@stanford.edu),  
Hyung Chul Ham (hchahm@kist.re.kr), and Suk Woo Nam (swn@kist.re.kr)

**Corresponding Author**

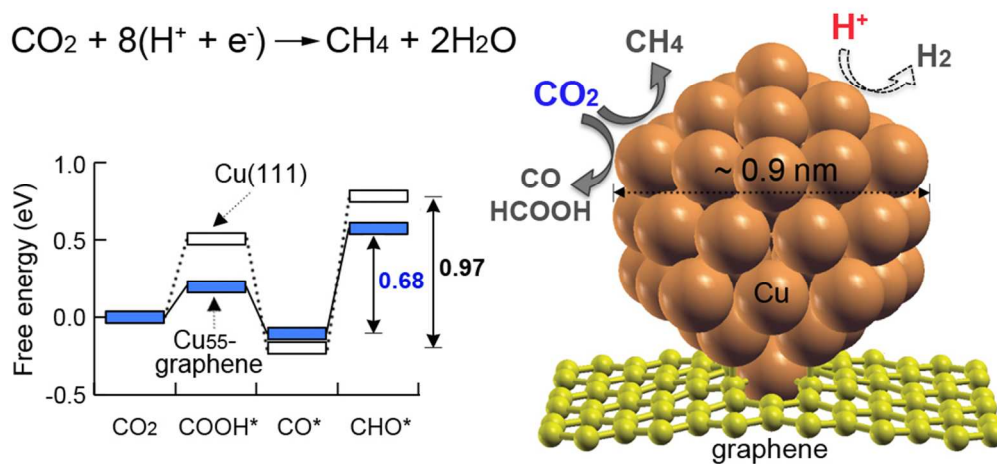
\*Dong-Hee Lim

Email: limkr@kist.re.kr, Phone: +82-2-958-5293, Fax: +82-2-958-5199

# ABSTRACT

Density functional theory studies demonstrate that defective graphene-supported Cu nanoparticles can modify the structural and electronic properties of copper for enhancing electrochemical reduction of carbon dioxide ( $\text{CO}_2$ ) into hydrocarbon fuels ( $\text{CH}_4$ ,  $\text{CO}$ , and  $\text{HCOOH}$ ). We not only provide improved understanding of  $\text{CO}_2$  conversion mechanisms on both Cu and the Cu nanoparticle system, but also explain a key factor for enhanced  $\text{CO}_2$  conversion. A promising catalytic material for  $\text{CO}_2$  conversion into hydrocarbon fuels may allow for geometry flexibility upon interaction with a key intermediate of  $\text{CHO}^*$ .

## Graphical Abstract



The electrochemical conversion of CO<sub>2</sub> to hydrocarbon fuels would not only assist in paving a path toward renewable energy, but also contribute to mitigating CO<sub>2</sub> emissions. The main challenge for advancing CO<sub>2</sub> reduction is to improve the energy efficiency of the process. Although both reasonably high current densities and moderate efficiencies have been achieved, they have not yet been achieved together.<sup>1</sup> Various metal-based catalysts (i.e., copper<sup>2-4</sup>, platinum<sup>5,6</sup>, iron<sup>7,8</sup>, nickel<sup>9,10</sup>, gold<sup>11-13</sup>) have been used to improve energy efficiency of the electrochemical reduction of CO<sub>2</sub>. Among them, copper has been widely accepted as a promising metal for CO<sub>2</sub> reduction due to its high ability to produce hydrocarbon fuels such as carbon monoxide (CO), formic acid (HCOOH), methane (CH<sub>4</sub>), and ethane (C<sub>2</sub>H<sub>4</sub>)<sup>3</sup>; however, the quantities of produced fuels are inefficient due to the large overpotential. According to experiment<sup>14</sup> and density functional theory (DFT) modeling investigations<sup>15</sup>, the production of CH<sub>4</sub> from CO<sub>2</sub> requires at least -0.8 V vs. RHE (i.e., reversible hydrogen electrode, in which the measured potential does not change with the pH). Hori *et al.*<sup>14</sup> pointed out that the electrochemical reduction of CO<sub>2</sub> is primarily hindered by a high overpotential, which results from the initial electron transfer to form the intermediate species, •CO<sub>2</sub><sup>-</sup>. Also, recent DFT studies of CO<sub>2</sub> electrochemical reduction have used CO and CHO intermediates as activity descriptors for CO<sub>2</sub> reduction to methane<sup>15-17</sup>, which is based on the fact that previous experimental studies<sup>18-20</sup> demonstrated that CO adsorption dominates on the electrode surface during CO<sub>2</sub> reduction.

Peterson *et al.*<sup>15,16</sup> demonstrated by conducting DFT studies that the key step in controlling the formation of hydrocarbons in the electrochemical reduction of CO<sub>2</sub> is the protonation of adsorbed CO\* to form the adsorbed CHO\* intermediate (such that, “\*”, denotes the adsorbed species and will be referred to thereafter). By increasing the stability of the CHO\* species relative to CO\*, it is expected that the energy efficiency of the electrochemical reduction of CO<sub>2</sub> would increase due to a significantly lowered overpotential. This may be achieved by utilizing nanostructures of copper supported on graphene. Changes in the lattice constant, surface stress and surface energy associated with the

nanoparticle size may improve the surface activity of copper for CO<sub>2</sub> reduction. Additionally, the unique electronic and physical properties of graphene would improve the CO<sub>2</sub> reduction kinetics, as it has been previously shown that graphene can enhance reaction kinetics on noble metal nanoparticles.<sup>21-25</sup> Also, carbon vacancies on graphene may significantly influence its physical and chemical characteristics and magnetic properties<sup>26-30</sup> and it can be used as anchoring points for the growth of metal nanoparticles, which will increase the durability of the Cu nanoparticle–graphene system and prevent sintering of the Cu nanoparticles.

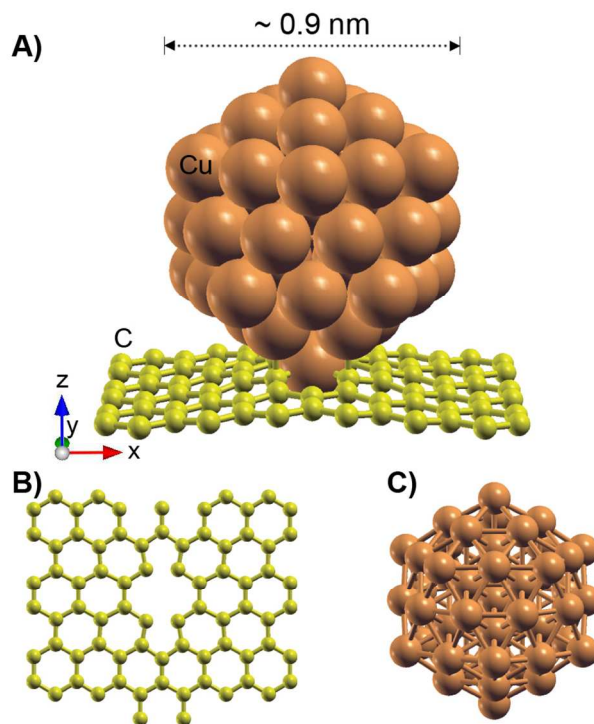
The current communication discusses improved catalysts for electrochemical CO<sub>2</sub> reduction to hydrocarbon fuels on Cu nanoparticles anchored at carbon vacancy sites of graphene. For this, free energies of the CO<sub>2</sub> reduction intermediates in electrochemical reaction pathways were calculated by using density functional theory (DFT) coupled with a computational hydrogen electrode (CHE) model suggested by Nørskov *et al.*<sup>15,31</sup>. Electron exchange-correlation functionals were represented with the generalized gradient approximation (GGA), and the model of Perdew, Burke and Ernzerhof (PBE)<sup>32</sup> was used for the nonlocal corrections. By employing the CHE model, a proton/electron (H<sup>+</sup> + e<sup>-</sup>) in solution can be indirectly treated and the effect of a bias can be applied by shifting  $\Delta G$  by  $+neU$ , where  $n$  is the number of proton-electron pairs transferred,  $e$  is the elementary positive charge, and  $U$  is the applied potential. The free energy change ( $\Delta G$ ) is calculated as  $\Delta G = \Delta E + \Delta ZPE - T\Delta S$ , where  $\Delta E$  is the total energy change directly obtained from DFT calculations,  $\Delta ZPE$  is the change in zero-point energies,  $T$  is temperature, and  $\Delta S$  is the change in entropy. Temperature is set to 18.5 °C to compare current DFT results with the experimental data of Hori *et al.*<sup>3</sup> Details of the free energy calculations including DFT total energies, ZPE, entropies, and free energies of the intermediates and the solvation energy correction are described in Supplementary Information Section 1.

Figure 1 depicts the Cu nanoparticle–graphene system consisting of an icosahedral Cu<sub>55</sub> nanoparticle (diameter of ~0.9 nm) adsorbed onto a 5-8-5 vacancy site of graphene (70 carbon atoms),

1 which is motivated by the magic numbers (13, 55, 147, etc)<sup>33,34</sup> of transition metal clusters providing a  
2 higher geometric or electronic stability compared to other cluster sizes. The Cu<sub>55</sub> nanoparticle shows a  
3 strong DFT adsorption energy of -4.26 eV, in which Cu is interacting with the dangling bonds of the  
4 neighboring carbons near the 5-8-5 vacancy site, which implies that the strong interaction may help to  
5 prevent sintering of the Cu nanoparticles. The size of the Cu nanoparticle used in the DFT calculations  
6 is smaller than those conventionally synthesized experimentally; however, considering the limitation of  
7 DFT calculations in terms of the system size that can be efficiently treated, Cu<sub>55</sub> is adequately large  
8 thereby minimizing the strong binding effect associated with highly undercoordinated Cu atoms that  
9 cause unrealistically high reactivity, thereby leading to an overestimation of overpotentials as was  
10 previously discussed in the work by Lim and Wilcox on the oxygen reduction reaction on Pt<sub>13</sub>-defective  
11 graphene.<sup>29,30</sup> In addition, the Cu nanoparticle size (~0.9 nm) may be plausible in electrochemical  
12 experiments as demonstrated in oxygen reduction reactions on graphene supported-gold cluster with  
13 diameters of approximately 1–2.5 nm (an average diameter of 1.8 nm)<sup>35</sup> and on graphene quantum dots-  
14 supported platinum nanoparticle with diameters of 2.2–3.3 nm (an average diameter of 2.8 nm).<sup>36</sup>

15

16



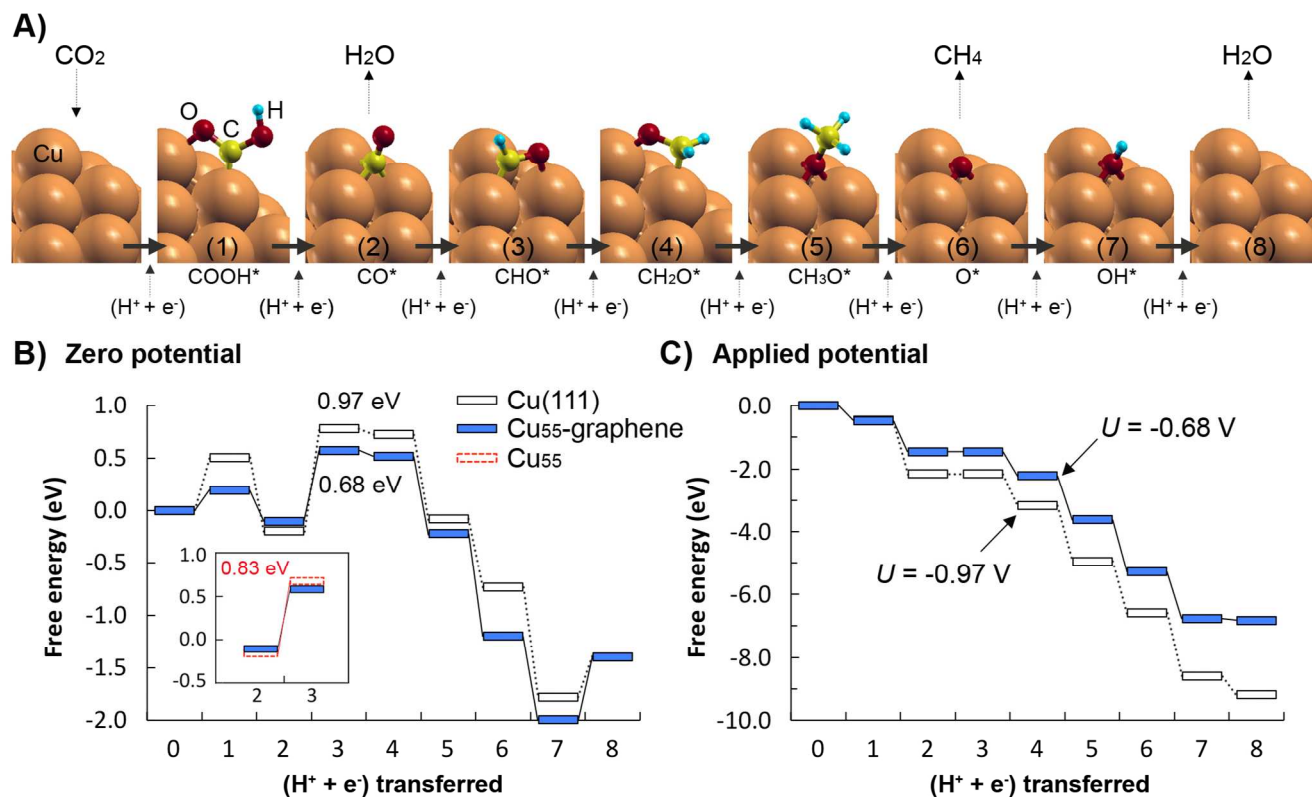
**Figure 1.** (A) Side view of  $\text{Cu}_{55}$  nanoparticle supported on defective graphene. (B) Top view of a 5-8-5 vacancy site of defective graphene with two missing C atoms at its center. (C) Icosahedral  $\text{Cu}_{55}$  nanoparticle. Brown and yellow colors represent Cu and C, respectively.

Figure 2 shows the lowest energy pathways of  $\text{CO}_2$  reduction on the  $\text{Cu}_{55}$ -defective graphene surface and a comparison of the  $\text{CO}_2$  reduction mechanisms between the Cu(111) (i.e., the most stable flat Cu surface among (100), (110), and (111) faces) and the  $\text{Cu}_{55}$ -defective graphene surfaces. Peterson *et al.*<sup>15</sup> extensively investigated the electroreduction of  $\text{CO}_2$  on a Cu(211) surface and determined the lowest energy intermediates. Based on this, we have examined three possible adsorption configurations for each intermediate and determined the lowest energy pathways as shown in Figure 2A. By transferring ( $\text{H}^+ + \text{e}^-$ ) from solution to an adsorbed species, a gas-phase  $\text{CO}_2$  molecule is converted to  $\text{COOH}^* \rightarrow \text{CO}^* \rightarrow \text{CHO}^* \rightarrow \text{CH}_2\text{O}^* \rightarrow \text{CH}_3\text{O}^* \rightarrow \text{O}^* \rightarrow \text{OH}^* \rightarrow \text{H}_2\text{O}_{\text{gas}}$ . The reaction intermediate configurations on the Cu(111) surface are also similar to those of Figure 2A (data not shown here).

At zero electrode potential ( $U = 0$  V) in Figure 2B, the Cu(111) surface shows the key energy barrier of 0.97 eV required for the protonation step of the CO species ( $\text{CO}^* \rightarrow \text{CHO}^*$ : (2)  $\rightarrow$  (3) in Figure 2B). This agrees reasonably well with the protonation step barrier of 0.74 eV on the Cu(211) step surface conducted by Peterson *et al.*<sup>15</sup>, which is due to the fact that a step-like surface of Cu(211) is more reactive toward binding adsorbates than a flat surface. In the Cu<sub>55</sub>-defective graphene system, reaction across the uncoordinated site significantly lowers the energy barrier of the key potential-limiting step to 0.68 eV; in other words,  $\text{CHO}^*$  becomes more stabilized relative to  $\text{CO}^*$  on the Cu<sub>55</sub>-defective graphene surface compared to on the Cu(111) surface. This implies that the Cu<sub>55</sub>-defective graphene system may help enhance the energy efficiency of the electrochemical reduction of CO<sub>2</sub> by lowering the key energy barrier. Instead, the Cu<sub>55</sub>-defective graphene system may hinder further reaction steps toward oxygen reduction due to an increased energy barrier associated with the proton/electron-transfer step of  $\text{OH}^*$  between steps (7) and (8) (i.e.,  $\text{OH}^* \rightarrow \text{H}_2\text{O}$ ) in Figure 2B. For this step, the Cu(111) surface requires 0.39 eV, while the Cu<sub>55</sub>-defective graphene system requires 0.60 eV. Considering the endothermic reaction steps of both systems in Figure 2B, the rate-limiting steps of the CO<sub>2</sub> reduction on the Cu(111) surface and Cu<sub>55</sub>-defective graphene system lie in the  $\text{CO}^* \rightarrow \text{CHO}^*$  step.

Figure 2C shows the CO<sub>2</sub> reduction mechanisms at applied electrode potentials of  $U = -0.97$  and  $-0.68$  V for the Cu(111) surface and the Cu<sub>55</sub>-defective graphene system, respectively. The applied potentials are required voltages for eliminating the energy barriers of the rate-limiting step ( $\text{CO}^* \rightarrow \text{CHO}^*$ ), which represents that the hydrocarbon CH<sub>4</sub>-forming reaction from CO<sub>2</sub> may occur at  $-0.97$  and  $-0.68$  V (*vs.* RHE) on the Cu(111) surface and the Cu<sub>55</sub>-defective graphene system, respectively. The DFT potential of  $-0.97$  V on the Cu(111) surface agrees fairly well with experimental measurements in which the formation of CH<sub>4</sub> from CO<sub>2</sub> on copper is initiated at about  $-0.8$  V and is maximized at about  $-1.0$  V at 18.5 °C.<sup>3,15</sup> An interesting finding is that the Cu<sub>55</sub>-defective graphene system requires

approximately 30 % less potential compared to the planar Cu(111) surface. Details of the CO<sub>2</sub> reduction reactions and free energy data are shown in Supplementary Information Section 2.



**Figure 2.** (A) The lowest energy pathways of CO<sub>2</sub> reduction on the Cu<sub>55</sub>-defective graphene. (B and C) Relative free energy diagrams without (B) and with (C) applied potential for CO<sub>2</sub> reduction on Cu(111) (empty rectangle with dashed lines), Cu<sub>55</sub>-defective graphene (filled rectangle with solid lines), and Cu<sub>55</sub> cluster (empty rectangle in the inset).

To understand in greater detail the reason for the smaller potential required for CH<sub>4</sub> formation on the Cu<sub>55</sub>-defective graphene system, the projected density of states (PDOS) of CO\*, CHO\*, and surface Cu atoms neighboring the adsorbates were analyzed by decomposing the electron density and wave function into the atomic orbital contributions. In Figure 3A, the Cu(111) surfaces with CO\* and CHO\* show hybridized *s*-, *p*-, and *d*-orbitals of Cu with *s*- and *p*-orbitals of the adsorbates between -6 and -12

eV. This phenomenon is also similarly shown in the case of the Cu<sub>55</sub>-defective graphene systems as indicated in Figure 3B. Both surface systems show strongly hybridized orbitals when CO is adsorbed; however, when CHO is adsorbed, the Cu(111) surface with the CHO\* intermediate species indicates relatively weaker hybridization while the Cu<sub>55</sub>-defective graphene system with CHO\* shows stronger hybridization between  $-8$  and  $-6$  eV and near the edge of the valence zone. This greater CHO-Cu overlap population on the Cu nanoparticle represents a relatively stronger stabilization of the CHO species on the Cu<sub>55</sub>-defective graphene system compared to the Cu(111) surface. Full details of each PDOS are shown in Supplementary Information Section 3.

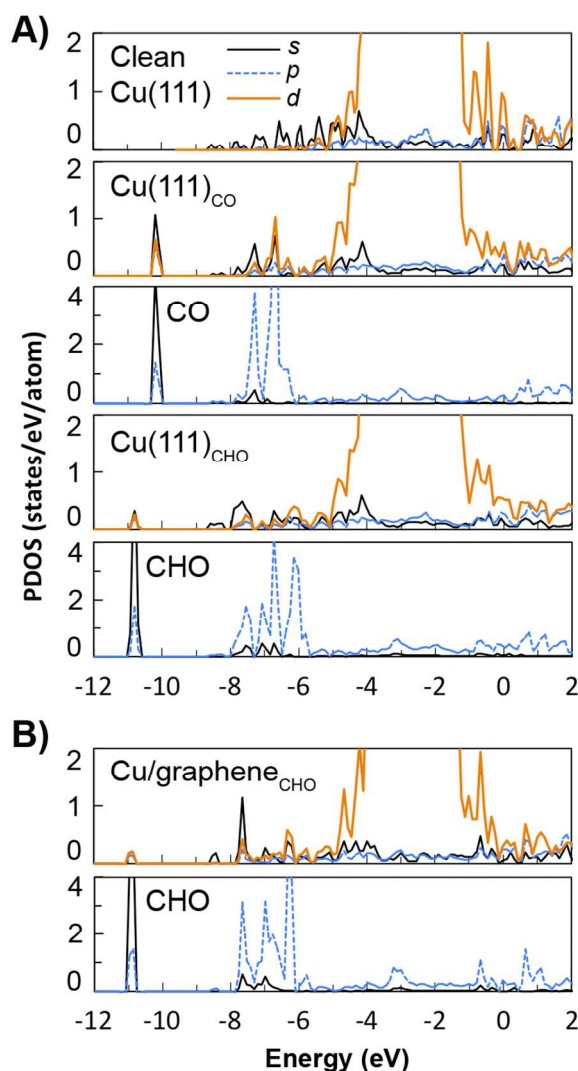


**Figure 3.** Projected density of states (PDOS) of the Cu(111) surface with adsorbed CO and CHO (A) and the Cu<sub>55</sub>-graphene surface with CHO (B). A system title of X<sub>Y</sub> indicates a surface (X) with adsorbed species (Y). Clean Cu, CO, and CHO represent clean Cu(111), adsorbed CO, and adsorbed CHO, respectively. The Fermi energy is referenced at 0 eV.

The stronger orbital hybridization between Cu and CHO on the Cu<sub>55</sub>-defective graphene system may be attributed to the advantage associated with graphene's unique electronic and physical properties as previously discussed. To confirm this, the key potential limiting step of CO\*→CHO\* was examined on a Cu<sub>55</sub> cluster without graphene as shown in the inset of Figure 2B. Without the graphene support, the energy barrier of the key step is 0.78 eV, demonstrating that the graphene support contributes to lowering the energy barrier of the key step from 0.78 to 0.63 eV by modifying the electron properties of the anchored Cu<sub>55</sub>. To better understand this, the *d*-band centers of Cu atoms were calculated. The *d*-band centers of all Cu atoms (or two Cu atoms where CHO\* is adsorbed) of the Cu<sub>55</sub> cluster and the Cu<sub>55</sub>-defective graphene are -2.24 (or -2.10) and -2.17 (or -2.07) eV, respectively. The higher shift of the *d*-band centers of the Cu<sub>55</sub>-defective graphene toward the Fermi level indicates the higher reactivity of Cu atoms resulting in an increase in the stability of adsorbates, which is attributed to the fact that an upshift of the *d*-band center causes the antibonding orbitals to shift higher, potentially making them more difficult to fill.

Also, another important factor for the stronger orbital hybridization between Cu and CHO on the Cu<sub>55</sub>-defective graphene system may be the geometry flexibility of the Cu nanoparticle. The geometry of the Cu nanoparticle is more flexible than that of the Cu(111) surface, which promotes CHO binding on the Cu nanoparticle by increasing the Cu-Cu distance when the CHO\* species is formed on the Cu nanoparticle surface. This is supported by the Cu-Cu distance measured at the CHO adsorbed site across both systems. The Cu-Cu distance of the Cu<sub>55</sub>-defective graphene system increases from 2.584

to 2.895 Å (12.1 % increase), while that of the Cu(111) surface is expanded from 2.571 to 2.683 Å (4.4 % increase) (see Supplementary Information Section 4). In other words, the geometry flexibility of the Cu nanoparticle has locally caused an expansive lattice strain effect, which in turn strengthens the Cu interaction with CHO species. This kind of strain effect is well known in metals or metal alloys in that an expansion in the lattice parameter can induce a shift in the *d*-band interaction toward the Fermi energy, resulting in strengthening the adsorbate interaction on catalytic surfaces.<sup>37</sup> Sakong and Gross<sup>38</sup> reported that the lattice expansive strain of copper surfaces (Cu(100), Cu(110), and Cu(111)) causes an upshift in the *d*-band centers. On the other hand, electronic ligand effects induced by the modification of electronic properties may have a minimal effect on the stability of the CHO\* intermediate species on both systems. This is because the PDOS of both clean systems are not significantly different as shown in Supplementary Information Section 3.

Furthermore, the reaction pathways toward the production of formic acid (HCOOH) and carbon monoxide (CO) gases are shown in Figure 4. HCOOH and CO gases are produced when the second proton and electron (i.e.,  $H^+ + e^-$ ) are transferred at steps 2(a) and 2(b) in Figure 4A and 4B, respectively. On the Cu(111) surface, the formation of both HCOOH and CO requires a potential of –0.51 V, by which the potential-limiting energy barriers at the first  $H^+ + e^-$  step are eliminated. This is in agreement with previous experiments<sup>14</sup> in addition to previous DFT studies<sup>15,16</sup> in that the formation of HCOOH and CO gases requires about –0.4 ~ –0.5 V (vs. RHE). The COOH\* species is more stable on the Cu<sub>55</sub>-defective graphene system compared to the Cu(111) surface for a similar reason as discussed previously with regard to the flexibility of the Cu nanoparticle geometry, resulting in limiting potentials of –0.19 and –0.39 V for the production of HCOOH and CO gases, respectively. This lower overpotential on the Cu<sub>55</sub>-defective graphene system may lead to the higher selectivity of HCOOH and CO compared to that on the Cu(111) surface.

In addition to the key rate-limiting steps of the protonation of adsorbed CO ( $\text{CO}^* \rightarrow \text{CHO}^*$ ) in  $\text{CO}_2$  reduction, the hydrogen evolution reaction (HER) significantly affects the electrochemical reduction of  $\text{CO}_2$  since HER is competitive against  $\text{CO}_2$  reduction. Effective  $\text{CO}_2$  reduction catalysts should show poor activity for the competitive HER.<sup>15-17</sup> In terms of the selectivity of  $\text{H}_2$  gas production, the  $\text{Cu}_{55}$ -defective graphene system shows a slightly poor activity for HER compared to the Cu(111) system as shown in Figure 4C, indicating limiting potentials of  $-0.22$  and  $-0.24$  V on the Cu(111) and  $\text{Cu}_{55}$ -defective graphene surfaces, respectively. In both cases, the potential limiting barriers for HER are present in the  $\text{H}_2$  gas desorption step ( $\text{H}^* + \text{H} \rightarrow \text{H}_{2(\text{gas})}$ ), which is attributed to the fact that atomic hydrogen adsorption is exothermic and its desorption is endothermic. The adsorption free energies of atomic hydrogen on the Cu(111) surface and  $\text{Cu}_{55}$ -defective graphene surfaces are  $-0.30$  and  $-0.32$  eV, respectively, which are comparative to the atomic hydrogen adsorption energy of  $-0.18$  eV on the Cu(111) surface<sup>17</sup> calculated using the GGA-PW91 functional. The predicted potential limiting step for HER in the current work agrees with previous DFT studies using a PBE functional and showing a potential of  $-0.1$  V on the Cu(211) step surface,<sup>15,17</sup> but the magnitude is different due to the stronger hydrogen adsorption at the fcc hollow sites of the Cu(111) surface. Note that the potential limiting step for HER may vary slightly depending on the DFT functional; for example, Peterson et al.'s work using the revised PBE (RPBE) functional suggests a limiting potential of  $-0.03$  V due to an endothermic adsorption of atomic hydrogen on the Cu(211) step site.<sup>15</sup> Nevertheless, we may conclude from Figure 4 that the  $\text{Cu}_{55}$ -defective graphene system promotes  $\text{CO}_2$  reduction into hydrocarbon fuels by lowering the rate-limiting energy barriers and relatively slightly inhibiting HER, at least showing similar selectivity of  $\text{H}_2$  compared to the Cu(111) surface.

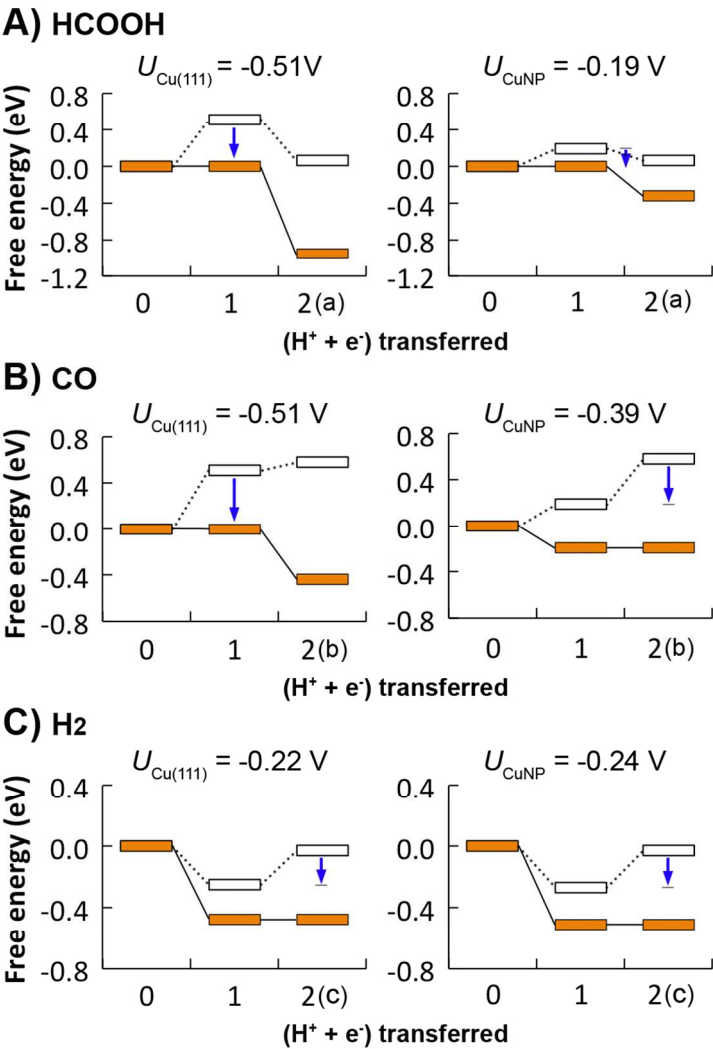


**Figure 4.** Relative free energy diagrams for HCOOH (A), CO (B), and H<sub>2</sub> (C) gas production on Cu(111) (left) and Cu<sub>55</sub>-defective graphene (right). Empty rectangles (with dashed lines) and filled rectangles (with solid lines) represent reactions without and with applied potentials. (H<sup>+</sup> + e<sup>-</sup>) transferred steps of 0 and 1 are the same steps as shown in Figure 2. The steps of 2(a), 2(b), and 2(c) represent HCOOH<sub>(gas)</sub> + surface, CO<sub>(gas)</sub> + H<sub>2</sub>O<sub>(gas)</sub> + surface, and H<sub>2(gas)</sub> + surface, respectively.  $U_{\text{Cu(111)}}$  and  $U_{\text{CuNP}}$  indicate necessary potentials to produce the gases on Cu(111) and Cu<sub>55</sub>-defective graphene, respectively. Arrows show the potential-limiting energy barriers that should be overcome for the gas production.

Lastly, it is worth noting the solvation effect in DFT modeling. Since an explicit treatment of a number of water molecules is still difficult to carry out using DFT, indirect methods may provide insight into better understanding the solvation effect. According to Peterson *et al.*'s solvation energy approximation on flat metal surfaces<sup>15,31,39</sup>, OH\*, R-OH\*, CO\*, and CHO\* gas-phase adsorbates may be stabilized in liquid water by approximately 0.5, 0.25, 0.1, and 0.1 eV, respectively. The current work employs this simple approximation for the adsorbed species and uses chemical potentials of the gas-phase molecules calculated in the work of Peterson *et al.*<sup>15</sup> where standard ideal-gas methods<sup>40</sup> were used to convert electronic energies of gas-phase molecules into chemical potentials at 18.5 °C (e.g., the free energy of liquid water was calculated as an ideal gas and adjusted to a fugacity of 3,534 Pa, which is the vapor pressure of water) (see Supplementary Information Section 1). If the solvation correction is not considered, the energy barrier of the first  $\text{H}^+ + \text{e}^-$  transfer step (i.e.,  $\text{CO}_2 \rightarrow \text{COOH}^*$ ) is overestimated resulting in the required potential of  $-0.76$  V for the HCOOH and CO formation on the Cu(111) surface, which does not agree with the experimental observation (between  $-0.4 \sim -0.5$  V).<sup>3</sup> Overall, the solvation energy correction lowers the reaction energy states and the reaction energy barriers become smaller; however, the relatively large solvation energy of OH\* causes an increase in the energy barrier for H<sub>2</sub>O desorption. In other words, the desorption energy of H<sub>2</sub>O from catalytic surfaces may be underestimated if the solvation effect is not taken into account. A detailed comparison between with and without solvation is provided in Supplementary Information Section 5.

## Conclusions

The current work provides theoretical evidence for improved CO<sub>2</sub> conversion into hydrocarbon fuels by using defective graphene-supported Cu nanoparticles. The results imply that an alternative catalytic material that allows for geometry flexibility upon interaction with adsorbates, especially with CHO\*, may improve CO<sub>2</sub> conversion into hydrocarbon fuels. A promising material may be Cu

nanoparticles supported on defective graphene as demonstrated here. In addition to the benefits of Cu nanoparticles, the defective graphene support may not only promote electron transport to the key potential limiting step species of CHO\*, but also help prevent sintering of Cu nanoparticles due to the strong anchoring nature of its defect sites. An improved understanding of CO<sub>2</sub> conversion mechanisms and the key factor regarding the geometry flexibility for the enhanced CO<sub>2</sub> conversion may help design promising materials for CO<sub>2</sub> conversion into hydrocarbon fuels. Also, future studies may need to focus on improving our understanding of solvation energies of COOH\* species showing the influence on HCOOH and CO gas production and its selectivity.

#### Corresponding Author

\*E-mail: limkr@kist.re.kr. Phone: +82-2-958-5293, Fax: +82-2-958-5199.

#### Acknowledgement

The current work is supported by the Basic Science Research Program through the National Research Foundation (NRF) of Korea funded by the Ministry of Education, Science and Technology (2012R1A6A3A04040490) and by the Supercomputing Center/Korea Institute of Science and Technology Information with supercomputing resources including technical support (KSC-2013-C3-017).

#### Supplementary Information Available

Details of DFT calculation methods, CO<sub>2</sub> reduction pathways, PDOS, and solvation effect diagrams are available via the Internet at <http://pubs.rsc.org>.

## Notes and references

- (1) Whipple, D. T.; Kenis, P. J. A., Prospects of CO<sub>2</sub> Utilization via Direct Heterogeneous Electrochemical Reduction. *J. Phys. Chem. Lett.* **2010**, *1*, (24), 3451-3458.
- (2) Hori, Y.; Kikuchi, K.; Murata, A.; Suzuki, S., Production of methane and ethylene in electrochemical reduction of carbon dioxide at copper electrode in aqueous hydrogencarbonate solution. *Chemistry Letters* **1986**, *15*, 897-898.
- (3) Hori, Y.; Murata, A.; Takahashi, R., Formation of Hydrocarbons in the Electrochemical Reduction of Carbon-Dioxide at a Copper Electrode in Aqueous-Solution. *Journal of the Chemical Society-Faraday Transactions I* **1989**, *85*, 2309-2326.
- (4) Dewulf, D. W.; Jin, T.; Bard, A. J., Electrochemical and surface studies of carbon-dioxide reduction to methane and ethylene at copper electrodes in aqueous-solutions. *J. Electrochem. Soc.* **1989**, *136*, (6), 1686-1691.
- (5) Sun, S. G.; Zhou, Z. Y., Surface processes and kinetics of CO<sub>2</sub> reduction on Pt(100) electrodes of different surface structure in sulfuric acid solutions. *Phys. Chem. Chem. Phys.* **2001**, *3*, (16), 3277-3283.
- (6) Kerbach, I.; Climent, V.; Feliu, J. M., Reduction of CO<sub>2</sub> on bismuth modified Pt(1 1 0) single-crystal surfaces. Effect of bismuth and poisoning intermediates on the rate of hydrogen evolution. *Electrochim. Acta* **2011**, *56*, (12), 4451-4456.
- (7) Takahashi, H.; Liu, L. H.; Yashiro, Y.; Ioku, K.; Bignall, G.; Yamasaki, N.; Kori, T., CO<sub>2</sub> reduction using hydrothermal method for the selective formation of organic compounds. *J. Mater. Sci.* **2006**, *41*, (5), 1585-1589.
- (8) Guan, G. Q.; Kida, T.; Ma, T.; Kimura, K.; Abe, E.; Yoshida, A., Reduction of aqueous CO<sub>2</sub> at ambient temperature using zero-valent iron-based composites. *Green Chem.* **2003**, *5*, (5), 630-634.
- (9) Pearce, D. J.; Pletcher, D., A study of the mechanism for the electrocatalysis of carbon-dioxide reduction by nickel and cobalt square-planar complexes in solution. *J. Electroanal. Chem.* **1986**, *197*, (1-2), 317-330.
- (10) Lee, E. Y.; Hong, D. W.; Park, H. W.; Suh, M. P., Synthesis, properties, and reactions of trinuclear macrocyclic nickel(II) and nickel(I) complexes: Electrocatalytic reduction of CO<sub>2</sub> by nickel(II) complex. *Eur. J. Inorg. Chem.* **2003**, (17), 3242-3249.
- (11) Hori, Y.; Kikuchi, K.; Suzuki, S., Production of CO and CH<sub>4</sub> in electrochemical reduction of CO<sub>2</sub> at metal-electrodes in aqueous hydrogencarbonate solution. *Chemistry Letters* **1985**, (11), 1695-1698.
- (12) Ohmori, T.; Nakayama, A.; Mametsuka, H.; Suzuki, E., Influence of sputtering parameters on electrochemical CO<sub>2</sub> reduction in sputtered Au electrode. *J. Electroanal. Chem.* **2001**, *514*, (1-2), 51-55.
- (13) Stevens, G. B.; Reda, T.; Raguse, B., Energy storage by the electrochemical reduction of CO<sub>2</sub> to CO at a porous Au film. *J. Electroanal. Chem.* **2002**, *526*, (1-2), 125-133.
- (14) Hori, Y.; Wakebe, H.; Tsukamoto, T.; Koga, O., Electrocatalytic process of CO selectivity in electrochemical reduction of CO<sub>2</sub> at metal-electrodes in aqueous-media. *Electrochimica Acta* **1994**, *39*, (11-12), 1833-1839.

- (15) Peterson, A. A.; Abild-Pedersen, F.; Studt, F.; Rossmeisl, J.; Nørskov, J. K., How copper catalyzes the electroreduction of carbon dioxide into hydrocarbon fuels. *Energy & Environmental Science* **2010**, *3*, (9), 1311-1315.
- (16) Peterson, A. A.; Nørskov, J. K., Activity descriptors for CO<sub>2</sub> electroreduction to methane on transition-metal catalysts. *Journal of Physical Chemistry Letters* **2012**, *3*, (2), 251-258.
- (17) Hirunsit, P., Electroreduction of Carbon Dioxide to Methane on Copper, Copper-Silver, and Copper-Gold Catalysts: A DFT Study. *Journal of Physical Chemistry C* **2013**, *117*, (16), 8262-8268.
- (18) Smith, B. D.; Irish, D. E.; Kedzierzawski, P.; Augustynski, J., A surface enhanced Raman scattering study of the intermediate and poisoning species formed during the electrochemical reduction of CO<sub>2</sub> on copper. *Journal of the Electrochemical Society* **1997**, *144*, (12), 4288-4296.
- (19) Ichinohe, Y.; Wadayama, T.; Hatta, A., Electrochemical reduction of CO<sub>2</sub> on silver as probed by surface-enhanced Raman scattering. *Journal of Raman spectroscopy* **1995**, *26*, (5), 335-340.
- (20) McQuillan, A. J.; Hendra, P. J.; Fleischmann, M., Raman spectroscopic investigation of silver electrodes. *Journal of Electroanalytical Chemistry* **1975**, *65*, (2), 933-944.
- (21) Kou, R.; Shao, Y.; Wang, D.; Engelhard, M. H.; Kwak, J. H.; Wang, J.; Viswanathan, V. V.; Wang, C.; Lin, Y.; Wang, Y.; Aksay, I. A.; Liu, J., Enhanced activity and stability of Pt catalysts on functionalized graphene sheets for electrocatalytic oxygen reduction. *Electrochemistry Communications* **2009**, *11*, (5), 954-957.
- (22) Seger, B.; Kamat, P. V., Electrocatalytically active graphene-platinum nanocomposites. Role of 2-D carbon support in PEM fuel cells. *Journal of Physical Chemistry C* **2009**, *113*, (19), 7990-7995.
- (23) Rao, C. V.; Reddy, A. L. M.; Ishikawa, Y.; Ajayan, P. M., Synthesis and electrocatalytic oxygen reduction activity of graphene-supported Pt<sub>3</sub>Co and Pt<sub>3</sub>Cr alloy nanoparticles. *Carbon* **2011**, *49*, (3), 931-936.
- (24) Seo, M. H.; Choi, S. M.; Kim, H. J.; Kim, W. B., The graphene-supported Pd and Pt catalysts for highly active oxygen reduction reaction in an alkaline condition. *Electrochemistry Communications* **2011**, *13*, (2), 182-185.
- (25) Yoo, E.; Okata, T.; Akita, T.; Kohyama, M.; Nakamura, J.; Honma, I., Enhanced electrocatalytic activity of Pt subnanoclusters on graphene nanosheet surface. *Nano Letters* **2009**, *9*, (6), 2255-2259.
- (26) Carlsson, J. M.; Scheffler, M., Structural, electronic, and chemical properties of nanoporous carbon. *Physical Review Letters* **2006**, *96*, (4), 046806.
- (27) Ma, Y.; Lehtinen, P. O.; Foster, A. S.; Nieminen, R. M., Magnetic properties of vacancies in graphene and single-walled carbon nanotubes. *New Journal of Physics* **2004**, *6*, (68), 68.
- (28) Lim, D.-H.; Negreira, A. S.; Wilcox, J., DFT studies on the interaction of defective graphene-supported Fe and Al nanoparticles. *Journal of Physical Chemistry C* **2011**, *115*, (18), 8961-8970.
- (29) Lim, D.-H.; Wilcox, J., DFT-based study on oxygen adsorption on defective graphene-supported Pt nanoparticles. *Journal of Physical Chemistry C* **2011**, *115*, (46), 22742-22747.
- (30) Lim, D. H.; Wilcox, J., Mechanisms of the Oxygen Reduction Reaction on Defective Graphene-Supported Pt Nanoparticles from First-Principles. *Journal of Physical Chemistry C* **2012**, *116*, (5), 3653-3660.

- (31) Nørskov, J. K.; Rossmeisl, J.; Logadottir, A.; Lindqvist, L.; Kitchin, J. R.; Bligaard, T.; Jónsson, H., Origin of the overpotential for oxygen reduction at a fuel-cell cathode. *Journal of Physical Chemistry B* **2004**, *108*, (46), 17886-17892.
- (32) Perdew, J. P.; Burke, K.; Ernzerhof, M., Generalized gradient approximation made simple. *Physical Review Letters* **1996**, *77*, (18), 3865-3868.
- (33) Sakurai, M.; Watanabe, K.; Sumiyama, K.; Suzuki, K., Magic numbers in transition metal (Fe, Ti, Zr, Nb, and Ta) clusters observed by time-of-flight mass spectrometry. *Journal of Chemical Physics* **1999**, *111*, (1), 235-238.
- (34) Lian, L.; Su, C. X.; Armentrout, P. B., Collision-induced dissociation of  $\text{Fe}_n^+$  ( $n=2-19$ ) with Xe: Bond energies, geometric structures, and dissociation pathways. *Journal of Chemical Physics* **1992**, *97*, (6), 4072-4083.
- (35) Yin, H.; Tang, H.; Wang, D.; Gao, Y.; Tang, Z., Facile Synthesis of Surfactant-Free Au Cluster/Graphene Hybrids for High-Performance Oxygen Reduction Reaction. *Acs Nano* **2012**, *6*, (9), 8288-8297.
- (36) He, G.; Song, Y.; Liu, K.; Walter, A.; Chen, S.; Chen, S., Oxygen Reduction Catalyzed by Platinum Nanoparticles Supported on Graphene Quantum Dots. *Acs Catalysis* **2013**, *3*, (5), 831-838.
- (37) Mavrikakis, M.; Hammer, B.; Nørskov, J. K., Effect of strain on the reactivity of metal surfaces. *Physical Review Letters* **1998**, *81*, (13), 2819-2822.
- (38) Sakong, S.; Gross, A., Dissociative adsorption of hydrogen on strained Cu surfaces. *Surface Science* **2003**, *525*, (1-3), 107-118.
- (39) Karlberg, G. S.; Wahnstrom, G., Density-functional based modeling of the intermediate in the water production reaction on Pt(111). *Physical Review Letters* **2004**, *92*, (13).
- (40) Cramer, C. J., *Essentials of Computational Chemistry Theories and Models*. 2nd ed.; John Wiley & Sons, Ltd.: West Sussex, England, 2004; p 355-366.